Received 30 April 2024; revised 21 June 2024; accepted 24 June 2024. Date of publication 26 June 2024;
date of current version 9 August 2024. The review of this article was arranged by Associate Editor F. Cruz-Roldan.

Digital Object Identifier 10.1109/OJSP.2024.3419563

Overview of the First Pathloss Radio Map Prediction Challenge

ÇAĞKAN YAPAR [1] (Member, IEEE), FABIAN JAENSCH[1], RON LEVIE[2], GITTA KUTYNIOK [3,4,5,6] (Fellow, IEEE), AND GIUSEPPE CAIRE [1] (Fellow, IEEE)

[1]Technical University of Berlin, 10623 Berlin, Germany
[2]Technion—Israel Institute of Technology, Haifa 3200003, Israel
[3]Ludwig-Maximilians-Universität München, 80331 Munich, Germany
[4]University of Tromsø, 9019 Tromsø, Norway
[5]Munich Center for Machine Learning, 80538 Munich, Germany
[6]DLR—German Aerospace Center, 82234 Weßling, Germany

CORRESPONDING AUTHOR: ÇAĞKAN YAPAR (e-mail: cagkan.yapar@tu-berlin.de).

An earlier version of this article was presented in part at the IEEE International Conference on Acoustics, Speech, and Signal Processing (ICASSP) in Rhodes, Greece, June 2023 [DOI: 10.1109/ICASSP49357.2023.10433928].

The work of Çağkan Yapar, Fabian Jaensch, and Giuseppe Caire were supported by BMBF Germany in the program of "Souverän. Digital. Vernetzt." Joint Project 6G-RIC under Project 16KISK030. The work of Gitta Kutyniok was supported in part by the Konrad Zuse School of Excellence in Reliable AI (DAAD), in part by the Munich Center for Machine Learning (BMBF), in part by the German Research Foundation under Grant DFG-SPP-2298, Grant KU 1446/31-1, and Grant KU 1446/32-1, in part by LMUexcellent (BMBF), in part by the Free State of Bavaria under the Excellence Strategy of the Federal Government and the Länder, and in part by Hightech Agenda Bavaria.

ABSTRACT Pathloss quantifies the reduction in power density of a signal radiated from a transmitter. The attenuation is due to large-scale effects such as free-space propagation loss and interactions (e.g., penetration, reflection, and diffraction) of the signal with objects such as buildings, vehicles, trees, and pedestrians in the propagation environment. Many current or planned wireless communications applications require the knowledge (or a reliable approximation) of the pathloss on a dense grid (radio map) of the environment of interest. Deterministic simulation methods such as ray tracing are known to provide very good estimates of pathloss values. However, their high computational complexity makes them unsuitable for most of the applications envisaged. To promote research and facilitate a fair comparison among the recently proposed fast and accurate deep learning-based pathloss radio map prediction methods, we have organized the ICASSP 2023 First Pathloss Radio Map Prediction Challenge. In this overview paper, we describe the pathloss radio map prediction problem, provide a literature survey of the current state of the art, describe the challenge datasets, the challenge task, and the challenge evaluation methodology. Finally, we provide a brief overview of the submitted methods and present the results of the challenge.

INDEX TERMS Challenge, dataset, deep learning, pathloss, radio map, received signal strength (RSS).

I. INTRODUCTION

In wireless communications, *pathloss* (or *large-scale fading coefficient*), quantifies the loss of wireless signal strength between a transmitter (Tx) and receiver (Rx) due to large scale effects. The signal strength attenuation can be caused by many factors, such as free-space propagation loss, penetration, reflection and diffraction losses by obstacles like buildings and cars in the environment. In dB scale pathloss amounts to $\mathrm{P_L} := (\mathrm{P_{Rx}})_{\mathrm{dB}} - (\mathrm{P_{Tx}})_{\mathrm{dB}}$, where $\mathrm{P_{Tx}}$ denotes the transmitted power at the Tx and $\mathrm{P_{Rx}}$ is the average received signal power, where the averaging is over a sufficiently large time, frequency, and space domain [2] spanning a few small-scale fading coherence interval in time, a few small-scale fading coherence bandwidths in frequency, and a few multiple of the carrier wavelength in space. In this way, the effects of the small-scale fading are averaged out and $\mathrm{P_L}$ captures only the large-scale effects. Notice that this local averaging is routinely performed by mobile devices when assessing their received signal strength (RSS), e.g. to calculate the so-called RSS indicator (RSSI) to inform the base station about the "quality" of their channel. A *pathloss radio map* provides pathloss value estimates on a fine spatial grid. Due to the local spatial

averaging mentioned above, the resolution of the spatial grid is tuned to accurately describe large scale effects, but sufficiently coarse to allow for local spatial averaging. For example, at a wavelength of 10 cm (carrier frequency of 3 GHz), a 1 m $\times$ 1 m grid may be a reasonable choice.

Many present or envisioned applications in wireless communications rely on the knowledge of the pathloss radio map of the area of interest, thus, accurately estimating pathloss is a crucial task. Some example use cases include: coverage map prediction [3], [4], [5], [6], user-cell site association [7], received signal strength (RSS) fingerprint-based localization [8], [9], [10], optimal power control [11], physical-layer security [12], activity detection [13], transmitter location selection [14], [15], [16], [17], optimal unmanned aerial vehicle (UAV) placement [18], spectrum sharing for joint communication and sensing [19], vehicle-to-vehicle (V2V) link scheduling [20], satellite-UAV on-demand coverage [21], beam alignment [22], path planning [23], access point (AP) switch ON/OFF strategy [24]. Establishing pathloss maps through measurement campaigns is a very labor-intensive and expensive enterprise. Therefore, the use of accurate deterministic simulations based on accurate propagation models such as ray tracing (which is based on a high-frequency approximation of Maxwell's equations) is considered a more feasible approach and is widely used. See Fig. 1 for some simulated radio map examples.

However, due to the high computational complexity of such simulations, they are not suitable for most of the intended applications of pathloss radio maps, while the conventional low complexity empirical methods are not capable of providing location-specific high fidelity pathloss predictions in complex propagation environments such as urban or indoor scenarios. Recently, many researchers, including the authors of the current paper [3], have presented deep learning-based pathloss radio map estimation algorithms that provide highly accurate pathloss map predictions, but with orders of magnitude lower computational time than conventional high-precision simulation methods, providing the fast and reliable pathloss radio map estimation required by applications. Some of the early work includes [3], [14], [15], [25], [26], [27].

By organizing this challenge, we have endeavored to provide an opportunity for a fair comparison of the recent neural network (NN)-based radio map prediction methods, based on the use of our publicly available *RadioMap3DSeer Dataset* [28] (cf. Section III-A and [29] for dataset descriptions).

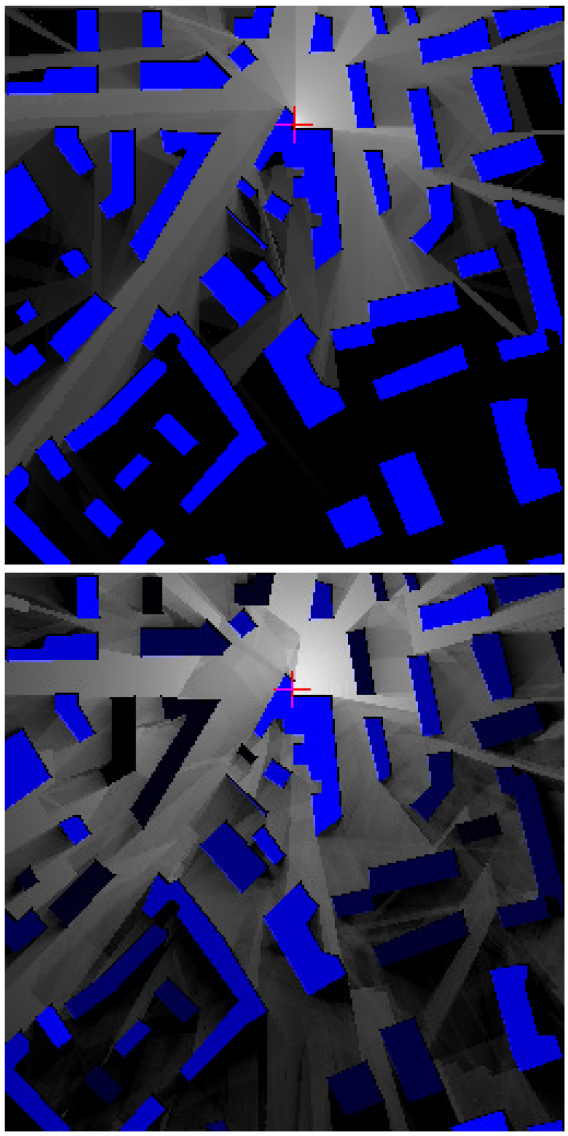

FIGURE 1. Examples of simulated pathloss radio maps for 2D and 3D settings. Tx positions are marked with a red plus sign. The intensity of the blue color indicates the height of a building; the stronger the color, the higher the building. The details of the system parameters corresponding to this figure are given in Section III-A. Top: 2D setting (ground level Tx placement). Bottom: 3D (rooftop Tx placement) setting used in the challenge.

II. OVERVIEW OF THE PREVIOUS WORK

In this section, we present an overview of pathloss radio map prediction methods by classifying them as either model-based or model-free (measurement-driven) or hybrid approaches. The focus is much more on the model-based and hybrid approaches because of their ability to exploit knowledge of the propagation environment and propagation physics (either by learning from synthetically generated data from highly accurate deterministic models, or directly from field measurements), resulting in higher accuracy than environment-agnostic model-free interpolation approaches.

A. MODEL-BASED PATHLOSS RADIO MAP PREDICTION

In the following, we first summarize the two traditional types of pathloss prediction models, namely the statistical and the deterministic ones [30], [31]. An important feature of model-based methods is that they do not rely on measurements at the time of deployment, which makes these methods the only option when, for example, Tx deployments at different locations are of interest, or a non-stationary Tx scenario is considered.

Afterward, an overview of deep learning-based methods follows, the subject of *The First Pathloss Radio Map Prediction Challenge*,[1] which have attracted increasing interest in recent years due to their ability to combine accuracy with computational efficiency. It was precisely these qualities that motivated us to organize this ICASSP Signal Processing Grand Challenge (SPGC).

1) STATISTICAL MODELS

Statistical (or *empirical*) *models* are primarily based on large scale measurement campaign data in specific propagation environments such as urban, suburban, rural scenarios. The measurements collected in specific environment types are used to derive environment type specific statistical relationships between pathloss and a few input parameters such as Tx-Rx distance, frequency, building density and line-of-sight/non-line-of-sight (LOS/NLOS) conditions in (sub)urban scenarios, while the fixed parameters of the models are determined by data fitting, i.e. they are chosen to maximize the agreement between the model prediction and the measurement data. Often, the error term between the model prediction and the measured data is attributed to shadowing loss due to signal penetration through obstructions in the environment and is then introduced as a random shadowing term in the final model equation.

Evidently, such models are not site-specific, i.e. they do not take into account the detailed specifications of the propagation environment of interest, i.e. the shapes and material compositions of the present objects, e.g. by taking them as input parameters, and here in this case of statistical models, rather they treat two different environments the same, as long as they fall into the same propagation environment category. Moreover, the position of Rx is often only important in terms of its distance from Tx, imposing a radial symmetry that does not hold in a real propagation environment with irregularly placed obstacles, or only roughly addressing the presence of obstacles by their proportion in the direct Rx-Tx path. Therefore, overall, these models have low accuracy in predicting pathloss at a given location.

Due to their simplicity, these models are computationally very efficient and have been used extensively in decision making problems where the actual position of an Rx is not important, but rather the distribution of pathloss for a given Tx-Rx distance and environment type.

Some popular statistical models include the log-distance [32], log-normal models [31], Okumura-Hata model [33], COST-231 model [34], Stanford University Interim model [35], Standard Propagation Model (SPM) [36] and QuadRiGa [37].

2) DETERMINISTIC MODELS

Deterministic models are based on the physics of electromagnetic wave propagation and are environment aware. Specifically, prominent deterministic propagation models, such as ray tracing [38] or finite-difference time-domain (FDTD) [39] simulations, are grounded in the physical principles of wave propagation and provide approximate solutions to Maxwell's equations, the first being based on high-frequency approximations and the second on discrete solutions of Maxwell's equations [30].

These models utilize detailed environmental information, including the shapes and locations of buildings and other objects such as vegetation, material properties and electromagnetic characteristics such as permittivity and conductivity, and antenna settings (e.g., location, azimuth, tilt, and radiation pattern) [27], [40], [41] to predict pathloss. By accurately modeling the physical mechanisms of electromagnetic wave propagation, such as transmission, reflection, scattering and diffraction, deterministic models offer the potential for highly accurate predictions, especially when accurate information about the geometry and material properties of the environment is available. Recent work such as [42] exemplifies the promising developments in obtaining accurate geometric and electromagnetic environment information and the resulting improvements in pathloss prediction by ray tracing over the use of less accurate environment information by validating with real-world measurements, demonstrating very good agreement between predictions and measurements.

Also, most commercial propagation simulation tools that employ deterministic models are validated by field measurements (as we mention for WinProp [43], which we used to generate the challenge dataset, in Remark 4), as a natural marketing requirement, since obviously no one would want to use a product that is not proven to work well.

In contrast to empirical models, deterministic models are site-specific (propagation environment, Tx characteristics and Rx location-aware) and adhere more closely to the principles of electromagnetic wave propagation, and therefore generally provide much more accurate results.

However, they typically consume large amounts of computational resources and are time intensive, making them prohibitively slow for many applications that require fast computation, such as real-time operations or large-scale, exhaustive predictions.

Among the well-known ray-based methods are the Shooting and Bouncing Ray (SBR) [44] and the Vertical-Plane-Launch (VPL) [45] methods [38]. Some widely employed accelerated (e.g., by space partitioning [46]) ray-based simulation approaches include the Dominant Path Model (DPM) [47] and Intelligent Ray Tracing (IRT) [48], the latter being our choice for preparing the datasets of the present challenge. A brief description of the IRT and how we chose its simulation parameters can be found in the Appendix.

Remark 1: We note that many deterministic models have parameters that can be calibrated by measurements, and the degree of dependence on such calibration measurements sometimes leads to classifying such methods as semi-deterministic, *especially when the deterministic physical model part is substantially simplified. One such example is*

[1] [Online]. Available: https://RadioMapChallenge.GitHub.io/

the DPM, where only the shortest (least attenuated) free space path is considered, which leads to the consideration of only diffractions and thus to the omission of reflections altogether, presumably reducing complexity without significantly compromising accuracy [47]. Among many, another notable example of semi-deterministic models is the widely used and improved Motley-Keenan multi-wall model [49], [50] specialized for indoor settings, which has been shown to provide relatively close pathloss prediction accuracy to more complex ray tracing methods.

3) DEEP LEARNING-BASED METHODS

In the following, we provide an overview of the deep neural network (DNN)-based methods that learn complex deterministic models and can provide highly accurate predictions, but in much less time than their deterministic model counterparts.

This approach, which has been the subject of numerous papers and of the SPGC presented here, has been shown to provide a very desirable trade-off between accuracy and computational time, drastically reducing the latter with respect to deterministic models without severely impairing the former, in contrast to statistical models.

a) Motivation and background: With the advent of realistic and large-scale data availability and computational power, recent years have witnessed the emergence and increasing interest in deep learning-based methods, which have also found profound impact on the pathloss radio map estimation problem.

Earlier work, however, did not yet benefit from efficient neural network designs and large, high-quality datasets with geometric environmental descriptions, and their improvements in accuracy over conventional methods are rather limited. In addition, these neural networks are only useful in the environment for which they are trained, i.e. they do not generalize to unseen environment maps, as a consequence of the fact that they are only trained to predict pathloss within a single environment.

For example, in [51], [52], the neural network is a function that returns an estimate of pathloss for each input Tx-Rx location. The network is trained on a fixed map and simulated pathloss values at a set of Tx-Rx locations. There are several other papers on pathloss prediction that use fully connected neural networks that do not consider the environment map information and use additional information such as the height of the transmitter/receiver or the distance between them. For example, see the survey [53] and the papers [54], [55], [56]. These methods are clearly unsuitable for predicting the radio map as a function of the environment map geometry given as input to the neural network.

Hence, these methods can also be regarded as non site-specific, similar to empirical models, since once trained in a certain environment, they do not generalize to other sites.

To the best of our knowledge, the first generalizable DNNs that can achieve high accuracy in unseen (not available in the training dataset) were RadioUNet [3], [26], proposed by the authors of the current paper, DA-cGAN [14], PLNet [27] and FadeNet [15]. These models learn to approximate the (predictions based on the) underlying electromagnetic propagation phenomenon by training on datasets that were generated by employing simulations based on high complexity deterministic models. Such methods take as input the Tx position map and the environment map(s), and thus learn to predict the pathloss radio map for any Tx position and for any environment map(s). The propagation environments considered have been of varying complexity. While the RadioUNet setting was 2D propagation (i.e., fixed Tx, Rx, and building heights) in urban environments with isotropic Tx, so that Tx location and building footprints can be described by black and white images as input features, more realistic complex settings (e.g., 3D propagation and evaluation settings, different material properties, directional Tx, beam patterns) have been considered in later work, leading to the use of many input features to describe the complex propagation environment and Tx characteristics.

Since these methods take essentially the same inputs to estimate radio maps as the deterministic models, high fidelity descriptions of the geometry and material properties of the environment are also very important [42].

On a modern graphics processing unit (GPU), a radio map prediction using such DNNs typically takes on the order of tens of milliseconds, which amounts to a 100× to 10,000× reduction in computation time, while the deviation of the model output from the prediction of the underlying simulation model is not large, as we also observe in the results of the challenge participants in Section VIII.

b) Overview of the Existing Work: RadioUNet [3] has two versions, RadioUNet$_C$ and RadioUNet$_S$, where the former falls into the setting of this section and takes the city environment map and the one-hot Tx location map to predict the pathloss radio map, while the latter takes pathloss measurements from the site of interest as an additional input feature. We call such methods that combine the learning of a propagation model with the use of measurements collected at the site of interest *hybrid approaches* and discuss them in Section II-B.

RadioUNet is a UNet [57] variant that cascades two UNets, resulting in a "W" shape. The input of the second UNet is the same as the input of the first UNet (city map + transmitter position as image), plus an additional feature channel, the output of the first UNet. The WNet (cascaded UNet) is trained in a curriculum. Initially, the first UNet is trained to estimate the ground truth pathloss maps from a large training dataset, which may represent reality in a coarser way than desired (for example, due to the difficulty of generating a large dataset for the desired setting, as noted in several papers such as [58], [59]). Then the weights of the first UNet are frozen and the second UNet is trained to estimate the pathloss maps.

The second UNet in the cascaded W structure was used to serve three different purposes: 1) reducing the size of the DNN compared to using only one large UNet, 2) estimating the coverage map, 3) adapting to more complex propagation

settings than the available large dataset used for training (*transfer learning* [60]) through the use of measurements (samples) collected from the complex setting of interest. The merits of this use case have recently been experimentally proven by measurements for the challenging case of directional Txs [61].

Other notable use cases of transfer learning were presented in PLNet [27], EM DeepRay [58], Radio DIP [59] and in [62], where the whole DNNs are further calibrated/fine tuned using the real world measurements (or their synthetic surrogates [3], [59]). Unlike RadioUNet [3] and [61], these models have no partial DNNs whose weights are frozen (first UNet in RadioUNet [3] and in [61]) during adaptation/calibration/fine tuning.

PLNet [27] is a single UNet and takes 8 input features, which are building, antenna height, frequency, antenna gain, tilt, azimuth, clutter and terrain, to provide the model with the ability to operate under variations of such realistic propagation settings. Most notably, the authors show that PLNet, trained on real field data, significantly outperforms ray tracing, indicating the ability of the DNN to learn a better mapping of the inputs to the pathloss radio map than ray tracing. PLNet is reportedly used by many field engineers.

FadeNet [15] also uses the UNet architecture and takes as input transmitter location (if not known to be fixed, omitted in this case), buildings, terrain, foliage, and LOS (binary, 1 if the grid point is in LOS, 0 otherwise) maps. The authors used synthetic data generated by ray tracing and data augmentation, the latter of which also proved useful in later work [4], [24], [41], [58], [63]. The authors also investigated the effect of the similarity of topographic features in the training and test sets and the size of the training dataset on prediction accuracy.

In [64], the authors considered a reflection-only scenario (no diffraction or penetration interactions of rays with buildings) generated by VPL [45] simulations in 2D settings, and a modified convolutional autoencoder framework involving ResNeXt networks [65], skip connections, and atrous/dilated convolutions [66], [67], the lastmentioned also proving very effective in later work [4], [41], [58], [68], [69]. The authors presented a stepped solution where identical but separate models are trained to iteratively predict each ray reflection.

In RadioTrans [70], [71], the authors augmented the convolutional encoder/decoder structure with transformer-based [72], [73] modules with the goal of learning the long-range spatial relationships between Tx, Rx pixels, and obstacles in the propagation environment. They supported the NN with an additional input, which they called Grid Anchor (GA), which involves the concatenation of grid coordinates and transmitter coordinates at all grid points. The use of this additional input feature has been found to be beneficial in other work as well [29], [41], [74].

Enhancements to the UNet for pathloss prediction were proposed in [75] by replacing the pooling layers with strided convolutions [76] and combining the UNet with inception modules as introduced by GoogleNet [77].

To the best of our knowledge, radio map prediction at numerous heights (3D prediction setting), was first proposed in DeepRay [68] and soon after in [78], by employing multiple output channels corresponding to the set of altitudes considered. More recently, the problem has been studied in detail in [79], where several DNN designs are compared and a 3D prediction radio map dataset is presented.

PPNet [80], which was partially adopted by the challenge method of the same name ([81], cf. Section VII-C), builds on the SegNet architecture [82], which involves a modification of the pooling method that stores the initial location of pixels in high-level feature maps and exploits these maps during the upsampling phase to achieve higher edge resolution prediction. Improvements in prediction accuracy were achieved by using a Gaussian kernel instead of a one-hot representation as the Tx input feature, and further by using a *Positional Encoding* input feature that conveys the spatial distance between the Tx location and the locations of the other points in the grid.

In EM DeepRay [58], the permittivity and conductivity of the walls in the indoor setting are considered as input features along with the Positional Encoding and the free space pathloss (FSPL) map, which is a function of distance and carrier frequency, allowing the model to perform well at different frequencies. The benefits of using such radially symmetric pathloss functions as input features have also been demonstrated in [5] and recently in [61], where the log-distance and 3GPP 38.901 UMa-NLOS models [83], respectively, were used to generate input coarse pathloss radio maps.

Remark 2: In DeepRay [68] and EM DeepRay [58], the Motley-Keenan multi-wall model [49], [50] was shown to yield not too inferior performance in comparison to uncalibrated ray tracing and the presented deep learning-based methods before calibration, while suffering from longer computation times than the deep learning-based method due to its usual non-parallelized implementation, i.e., pathloss for each pixel is computed serially, as we also observed in the implementation of a baseline tomography method *in our RadioUNet paper [3]. We would like to point out that an efficiently parallelized GPU-enabled computation of such algorithms might be feasible, e.g. as was showcased by one of the challenge teams [24], [84] in calculating their fractional LOS maps using the CuPy library [85]. Although methods such as the Motley-Keenan multi-wall model and* direct path model *[86], [87] yield inferior prediction accuracy compared to deep learning-based methods trained on large training data (and potentially further improved by calibration/fine tuning with measurement data), the acceleration of former methods may still make them attractive, because of the possibly higher accuracy of using such methods in the small data regime where DNN based methods cannot perform well due to lack of sufficient training data. Moreover, the use of radio maps generated by such methods as input features to pathloss radio map prediction DNNs has also proven very useful [88].*

Nevertheless, given the relatively easy access to high computing power available today, we believe that the generation of large synthetic datasets (based on accurate deterministic

models) is an effort that can be accomplished with relatively modest investments, which helps immensely in achieving very high accuracy, through the use of DNNs.

PMNet [4], whose modified version ([89], cf. Section VI-I-B) performed best in the challenge, is an encoder-decoder DNN where the encoder contains a series of ResBlocks [90] and applies multiple parallel atrous convolutions at different rates [67], [91] and uses skip connections across the layers of the encoder and decoder. Each ResNet [65] layer consists of several bottleneck layers comprising convolution, batch normalization, and rectified linear unit (ReLU).

The effect of building density was studied in the challenge (Agile method [84], cf. Section VII-A) follow-up paper REM-U-Net [24]. The advantages of the use of the fractional LOS map (somewhat similar to the direct path model [86], [87]), were demonstrated over the conventional LOS map. The authors developed several algorithms to generate their fractional LOS maps. They also studied the application of pathloss radio maps to the AP ON/OFF switching problem [92] as a novel application of radio maps.

In [41], the authors presented a comprehensive radio map dataset generated by ray tracing simulations with directional antennas using environmental information taken from the real world, including trees and realistic building heights with approximated roof shapes, as well as aerial imagery of the same locations. The use of deformable convolutional layers [93] was proposed and numerical experiments were performed with different DNN architectures and with different ways of encoding the city geometry and with aerial imagery.

In DA-cGAN [14], the authors proposed to use conditional generative adversarial networks (cGAN) [94] for indoor radio map prediction in parallel with optimal Tx placement while taking into account the interference from the outside macro-cell Txs. They introduced appropriate loss functions and a two-stage training strategy. To better learn the propagation patterns, they proposed the gradient similarity (GSIM) index, a metric that measures the gradient pattern between two images rather than the sole pixel-wise match. The authors also reported a positive impact of training their model in the cGAN framework, which uses a discriminator architecture.

In [95], the authors considered the application of cGANs to the outdoor scenario using the *RadioMapSeer Dataset* introduced in [3], [29]. The authors also report on the beneficial effects of the discriminator network and their numerical experiments show that their approach provides better prediction accuracy than RadioUNet [3] and is of lower computational complexity.

In PL-GAN [63], the authors presented a generative adversarial network (GAN)-based approach to predict pathloss of an outdoor urban envrinmont directly from satellite images or the height map of the region. They concluded that height maps produce better results because the actual height profile is more informative about the shadowing effects compared to satellite imagery.

The authors of IRGAN [69] proposed cGAN-based DNNs for an indoor scenario involving materials with different electromagnetic properties. They presented a segmentation model to extract doors, interior walls, and exterior walls from raw floor plan images. The pixels corresponding to each material are encoded by the value of their permittivity, and the thickness of the walls is also taken into account. They improved their method by using the attention mechanism [72] and dilated convolutions [67].

In RADIANCE [40], the authors considered the indoor setup with varying carrier frequencies, material types, and notably, antenna patterns represented by the antenna gain values for various azimuth and elevation angles. They used a gradient-based loss function that calculates the magnitude and direction of change in RSS/pathloss at each grid point, similar to GSIM in [14], and employed a PatchGAN [96] discriminator with instance normalization.

Remark 3: We would also like to point out the efforts to efficiently parallelize highly complex ray tracing algorithms such as SBR [44]. For example, in a recent paper [97], the authors report that they reduced the computation time for 100,000 rays from 852 seconds to 1 second compared to serial computation, and for 1,600,000 rays from 86,214 seconds to 6.5 seconds, a remarkable 13,263-fold speedup. We would like to remind that the typical computation times achieved by DNN-based methods are in the order of tens of milliseconds, and therefore DNN-based methods seem to be more suitable for applications that require fast predictions. Moreover, as shown in PLNet [27], DNN-based methods trained on field data can outperform a ray tracer (although compared to only one ray tracing software).

Overall, we hope that all of these developments can synergize to further reduce computation time and increase accuracy.

B. HYBRID APPROACHES

Hybrid approaches use both the propagation pattern relevant environment information, i.e. shape and material properties of the present objects, and optionally information about Tx such as its position, and measurement data (recall that the aforementioned model-based approaches do not rely on measurements in inference phase).

An early example of such a method was our measurement-assisted RadioUNet$_S$ [3], which incorporates measurements from the environment of interest as an additional input channel along with the environment map and the one-hot Tx position map into the framework of the general RadioUNet model (cf. Section II-A3b), thereby increasing the accuracy of the radio map estimation.

Such an approach is useful when the environment map given as an input feature channel does not represent reality with high degree of fidelity, or when the simulation method used to generate the training dataset is not highly accurate. Therefore, the network learns a hybrid of a radio map estimation method based on the given map, which is not completely reliable, and an interpolation method of the accurate pathloss measurements. In this scenario with inaccurate maps, a perturbed version of the ground truth maps is given as input to the

UNet. We considered three types of inaccuracies: 1) the map is given with one to four missing buildings; 2) the map is given without cars, but the ground truth simulation is computed with the cars; 3) training is done against simulations that are rather coarse approximations of reality.

In [98], the authors considered the problem of power spectral cartography, which can be viewed as RSS estimation in a given frequency band. The authors adopted a supervised inpainting learning approach by using completion autoencoders. The presented method takes measurements, a mask indicating the locations of the measurements on the grid, and the building map as input. A multi-emitter setting was considered, where the power measurements are assumed to be the sum of the powers of the signals emitted by each Tx.

In [99], the authors considered the single frequency multi-emitter scenario. They proposed not only to feed the measurement information and the environmental information consisting of the building map and the mask together as input, but to provide the encoder/decoder parts with the copies of the input measurement and/or environment information, which led to performance improvements especially at relatively high sampling rates. They further suggested to equip the autoencoder with skip connections, which outperformed the vanilla autoencoder and the proposed dual path autoencoders without skip connections. The numerical results showed that the skip-aided autoencoders with or without the dual path structure performed very similarly.

A UNet architecture taking a 3D building map and measurements as input was adopted in [100]. Two separate but identical UNets are trained to learn the mean and variance parameters, assuming that the RSS at each location is an independent Gaussian random variable. The variance map is considered to quantify the uncertainty, and inference is based solely on the output of the mean UNet. The papers on the Agile method [24], [84] of the challenge also reported that the use of this Gaussian modeling along with the use of KL loss resulted in better performance.

An earlier (to the best of our knowledge, the first) application of the hybrid approach based on deep learning to radio map estimation was the SS-GAN [25], where the authors recognized the importance of environmental information such as buildings and terrain. In their proposed GAN-based architecture, the environment and measurement maps are subjected to separate feature extraction layers, and the obtained feature vectors are concatenated to be further processed through learnable layers and upsampled to give an estimate of the radio map. Due to the non-availability of large datasets for training, the authors proposed to incorporate self-supervised learning. The performance of the proposed method was evaluated on a real-world 4G LTE dataset.

RME-GAN [5] considered the 2D setting and cGAN architecture to estimate pathloss from Tx position, building map and measurements inputs. The proposed method first used the log-distance pathloss model to obtain a rough estimate. Then, a two-stage training procedure was used where the first stage focuses on learning global propagation patterns and the second stage is dedicated to learning the details. A number of loss functions were considered for the different stages. The authors considered different sampling strategies to demonstrate the high generalizability of the proposed method. Numerical comparisons with several baselines were provided.

In EME-GAN [101], the authors used the cGAN architecture to estimate indoor RSS radio maps using measurements and a building infrastructure map as inputs, where the latter includes material types in the floor plan and no Tx positions were required during inference. Through numerical experiments, the good performance of the proposed method is demonstrated, outperforming their previous UNet-based method EME-Net [102] when sufficient number of measurements are available, while in low sampling rate regime, EME-Net [102] turned out to perform better.

In ACT-GAN [103], the authors considered three different settings. The first involved predicting radio maps using transmitter and building map information, as discussed in Section II-A3. The second scenario incorporated measurements into the previous setting, as described earlier in this section. The third scenario dealt with an unknown Tx position, where estimating its location was posed as a problem. The proposed DNN makes use of convolutions, convolutional block attention modules [104], aggregated contextual transformations [105], and uses the PatchGAN [96] discriminator. Numerical comparisons with previous work demonstrated the high accuracy of the proposed methods.

In [106], the authors proposed a cGAN-based method for radio map estimation using measurements and building map as inputs. The authors demonstrated the effectiveness of their method in handling inaccurate building map information, even when certain or random number of buildings are missing in the input. Although the proposed method does not consider Tx information, it still demonstrates competitive performance compared to Tx position-aware (but not measurement-aided) RadioUNet$_C$ (cf. Section II-A3b) [3].

C. MODEL-FREE PATHLOSS RADIO MAP PREDICTION

Model-free (or *interpolation*) methods are purely measurement driven and do not use any information about the environment or the Tx(s). As a result, such methods struggle to demonstrate high performance in cluttered propagation environments, such as urban and indoor environments, where the exact positions and material properties of obstacles have a profound effect on electromagnetic wave propagation.

The model-free approaches therefore impose some other assumptions, such as smoothness or a low-rank property. Some prominent interpolation methods include Radial Basis Functions (RBF) interpolation [107, Sect. 5.1], Kriging [108], tensor completion [109], and k-nearest neighbors Gaussian process regression [110].

For more information on model-free methods, please refer to the survey papers [111], [112] and the references therein.

In the following, we would also like to present some measurement-only DNN-based methods that have been published recently.

In [113], the authors demonstrated how to build a large indoor radio map dataset and proposed the use of a modified UNet architecture for interpolation, where the model takes only sparse measurements as input. Numerical and field experiments demonstrated that the proposed method outperforms a Gaussian process-based baseline [114] and is more robust to measurement location errors than the considered baseline.

For the multi-emitter power spectral cartography problem, the authors of [115] proposed autoencoder-based methods to complete the individual radio maps (which requires the estimation of the number of Txs), which resulted in a better estimation accuracy than operating directly on the aggregated map [98]. The proposed methods take the measurements and the measurement mask as input, i.e., the building input could apparently be omitted without performance degradation. Experiments with both synthetic and real data were used to evaluate the performance of the proposed algorithms.

In DeepREM [6], the authors considered the multi-emitter RSS radio map estimation problem and studied the performance of UNet and cGAN to estimate the radio maps using only the measurements. They presented their corresponding dataset and evaluated the performance of the studied methods in several scenarios. The numerical experiments demonstrate that UNet performs better when the test scenario aligns with the training data distribution, whereas cGAN is more effective when the discrepancy between the training and test scenarios is high.

In IRDM [116], the authors applied generative diffusion models [117] for interpolation of pathloss radio maps. They utilized a multi-stage training strategy and data augmentation. The authors noted certain limitations introduced by the use of denoising diffusion probabilistic models, namely, the requirement for a large number of refinement steps, which can make the method relatively slow.

III. DATASETS

A. TRAINING DATASET - RADIOMAP3DSEER DATASET

For training, we provided the challenge participants with the RadioMap3DSeer Dataset, which we made publicly available [28] as part of a collection of radio map datasets that we generated under various settings [29]. The RadioMap3DSeer takes into account different building heights and Tx deployment on rooftops of relatively high buildings (in comparison to other buildings in the city map).

The RadioMap3DSeer Dataset was intended to represent cellular network scenarios, and a natural use case of it is to serve as a training dataset for learning methods that predict pathloss from input city maps and Tx locations, the very task of the present challenge.

The pathloss radio maps of the dataset were generated based on the Intelligent Ray Tracing (IRT) [48] simulations with a maximum of 2 interactions (cf. Appendix) performed by the radio propagation modeling software *WinProp from Altair* [43], on a large collection of city maps, which were obtained from *OpenStreetMap* (OSM) [118] from the city maps of Ankara, Berlin, Glasgow, Ljubljana, London, and Tel Aviv, amounting to 701 city maps of size 256 m $\times$ 256 m. All simulations were run at a resolution of 1 meter and saved as images of 256 $\times$ 256 pixels in `.png` format. 80 rooftop transmitter locations per map were considered, resulting in a total of 56080 simulations. Pathloss values were simulated at a height of 1.5 m above the ground.

Remark 4: The high accuracy of IRT simulations with WinProp has been demonstrated by validation with field measurements in many cities such as Helsinki, Munich, Nancy, and Stuttgart, see e.g. [119] or [120] and the references therein.

Since the building height information provided by OSM [118] is often inaccurate (often giving constant height values, hence the use of such maps leads to predictions with large inaccuracies, as exemplified in [61]), we decided to assign random building heights by considering a reasonable range of heights to show the proof of concept. Each building in a city map was assigned a height in the range from 2 to 6 stories, where a story is regarded as 3.3 m. This range of 13.2 m (from a minimum of 6.6 m to a maximum of 19.8 m) is divided into 255 levels of equal length, and building heights are found by uniformly selecting one of these levels. This data is provided as two image sets in 8-bit `.png` format, one as black and white (BW) images of the pixels occupied by buildings (pixel value 255 if it belongs to a building, 0 otherwise), and one with their height encoded as gray levels 1-255 as explained above. The corresponding polygons with heights[2] are provided in `.json` format. All buildings are assumed to have the same generic material property.

Tx positions of the pathloss radio map simulations were generated on the buildings with a height of at least 5 stories (16.5 m). The transmitters were placed close to the edges to emulate a realistic deployment. The transmitter height from the rooftop was set to 3 m. We have restricted the Tx to be positioned within the 150 $\times$ 150 area in the center of the 256 $\times$ 256 city map if possible, and considered a larger area of 230 $\times$ 230 for the city maps with no buildings within the 150 $\times$ 150 area in the center. In the dataset, Tx positions are provided as one-hot images, where the pixel of the Tx is set to white, and the rest of the image is black. Similar to the height encoding in city maps described above, we also provided height-encoded Tx images where only the pixel of the Tx has a non-zero value. The value of this pixel was set as the height-encoding value of the building on which the Tx is placed. In addition, the Tx coordinates are provided as `.json` files.

The results of the IRT simulations are provided as 8-bit `.png` image files, which were obtained by post-processing of the simulation results by first converting the pathloss values

[2]Note that the building objects we generate are based on the footprints imported from OpenStreetMap [118] and the heights we assign to them, i.e., only horizontal flat roofs and vertical walls are considered.

TABLE 1. Parameters of the RadioMap3DSeer Dataset

Parameter	Value
Radio map size	256^2 pixels
Pixel length	1 meter
Rx height (receiving points in the sims.)	1.5 meters
Noise power spectral density (N_0)	−174 dBm/Hz
Transmit power (P_{Tx})	23 dBm
Antenna type	Isotropic
Height range of the buildings	6.6–19.8 meters
Tx height	3 m above a rooftop
Center carrier frequency	3.5 GHz
Channel bandwidth (W)	20 MHz
Noise figure (NF)	13 dB
Max PL in simulations/dataset ($P_{L,max}$)	−75 dB
Min PL in the simulations	−162 dB
PL threshold ($P_{L,thr}$)	−111 dB
PL range ($P_{L,max} - P_{L,thr}$)	36 dB
Simulation type	IRT
Max no. of interactions in IRT	2
Tile length in IRT simulations	10 meters
Simulations with cars in the map	No

P_L to pixel values between 0 and 1 by

$$p = \max\left\{\frac{P_L - P_{L,thr}}{P_{L,max} - P_{L,thr}}, 0\right\}, \quad (1)$$

where $P_{L,max}$=-75 dB denotes the maximum pathloss in all radio maps (the value at an Rx next to a Tx pixel with a height of 19.5 m. Note that the maximum is −75 dB, because the software averages over the 1 m^2 pixels and the Txs are placed 3 m above tall buildings with a minimum height of 16.5 m) in the dataset and $P_{L,thr}$ is the pathloss threshold, below which the received signal power is assumed to be not large enough for successful detection [3], [29], i.e., it is below the noise floor. In mathematical terms, we are interested in the pixels with the received signal power $(P_{Rx})_{dB} = P_L + (P_{Tx})_{dB}$ above the noise floor $(\mathcal{N})_{dB}$, i.e. the positions in the pathloss simulations where $(P_{Rx})_{dB} \geq (\mathcal{N})_{dB}$ holds, where $(\mathcal{N})_{dB} = 10\log_{10} WN_0 + NF$ is the noise floor in dB, with NF being the noise figure, W the signal bandwidth and N_0 the thermal noise power spectral density. Solving this for pathloss P_L we get the *pathloss threshold* $P_{L,thr}$ as $P_L \geq P_{L,thr} = -(P_{Tx})_{dB} + (\mathcal{N})_{dB}$. For the parameters of the dataset in Table 1 we found $P_{L,thr}$=-111 dB. Overall, after the post-processing of a pathloss simulation by (1), the pixels with pathloss values below the noise threshold are set to 0, and high pathloss values (high received signal powers) in simulations obtained high values in pathloss radio maps, e.g. an Rx pixel next to a Tx pixel of minimum height (placed 3 m above on a 16.5 m tall building) has the maximum value of 255 in a post-processed radio map presented in the RadioMap3DSeer Dataset.

We would like to point out that over-the-rooftop propagation from a Tx placed on a relatively tall building (3D setting considered in the RadioMap3DSeer) will reach greater distances than a Tx at ground level of 1.5 m (2D setting), and together with the varying building heights, such placement gives rise to richer and more complicated pathloss patterns compared to ground level Tx deployment, see Fig. 1. For the radio map in the 2D setting in Fig. 1, the center carrier frequency was set to 5.9 GHz. $P_{L,max} = -47$ dB and $P_{L,thr} = -147$ dB were found and used to scale the simulated values to the pixel values by (1) as described above. All buildings were set to a height of 25 m.

A snapshot from a simulated pathloss radio map by WinProp and the rays for a receiver pixel in the adopted 3D setting are shown in Fig. 2(a). The entire simulated pathloss radio map of this area of 256 m × 256 m is shown in Fig. 2(b). Fig. 2(c) shows the corresponding pathloss radio map in the RadioMap3DSeer Dataset after the post-processing described above. The corresponding 2.5D and 2D (BW) city maps are shown in Fig. 2(e) and in (d), respectively.

B. TEST DATASET

To evaluate the participants' methods, we prepared a test dataset that was not previously published. 84 city maps of the same size of 256 m × 256 m were taken from OpenStreetMap [118] in Istanbul, resulting in 6720 (84 maps × 80 Tx per map) pathloss simulations. The same dataset generation procedure and simulation parameters were used as for RadioMap3DSeer Dataset as described above.

IV. THE CHALLENGE TASK

The task of the challenge was to predict the pathloss radio map given the city map and the transmitter location, i.e., the same task and input setting of deterministic simulation methods such as ray tracing (cf. Section II-A3).

The participants were allowed to design their input features (i.e. pre-processing) freely, as long as the test run-time of the proposed method was orders of magnitude lower than the pathloss simulation by the propagation modeling software.

V. EVALUATION METHODOLOGY

Participants were asked to submit their radio map predictions for the challenge test set (sent to them without ground truth) along with the code that runs the evaluation.

When assessing the prediction performance of the presented methods, we first set the pixels of the radio map predictions known to be occupied by the buildings to zero, i.e., since the ground truth value at such pixels is zero, the prediction error for such pixels was guaranteed to be zero.

We evaluated the accuracy of the submitted methods by the root mean square error (RMSE)

$$\text{RMSE}_{\mathcal{T}} = \sqrt{\frac{1}{|\mathcal{T}|}\sum_{n\in\mathcal{T}} \text{RMSE}(n)^2} \quad (2)$$

where $\mathcal{T}$ is the test set and RMSE(n) is the RMSE for the radio map n, defined as

$$\text{RMSE}(n) = \sqrt{\frac{1}{RC}\sum_{i=1}^{R}\sum_{j=1}^{C}\left(\tilde{P}_L^{(n)}(i,j) - P_L^{(n)}(i,j)\right)^2} \quad (3)$$

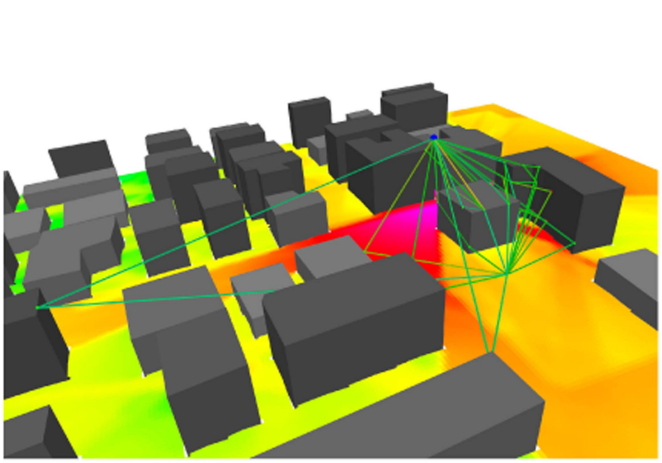

(a) An IRT radio map simulation for the RadioMap3DSeer Dataset.

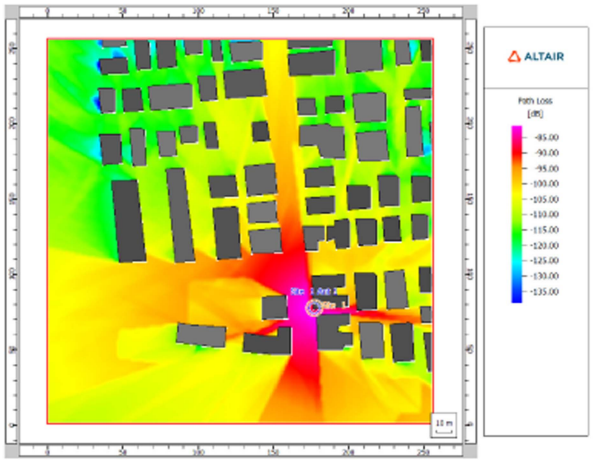

(b) Bird's-eye view of the radio map simulation in (a).

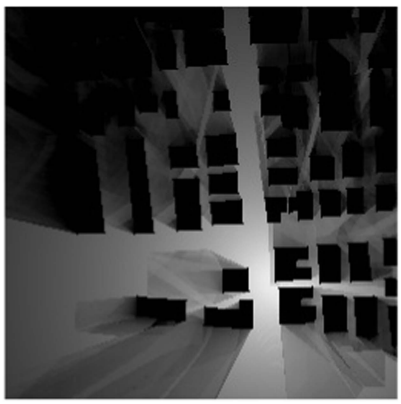

(c) Pathloss radio map

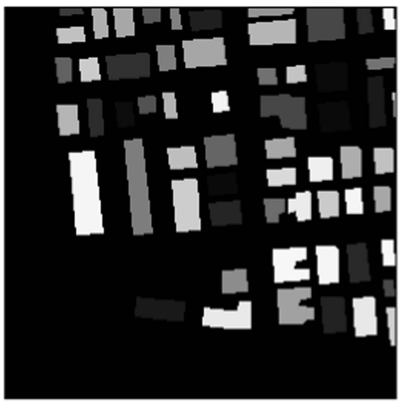

(d) City map with encoded height

(e) City map w/o height (BW)

FIGURE 2. **(a) A snapshot of a WinProp IRT simulation showing the rays reaching a selected location on the grid. (b) The bird's eye view of the simulated pathloss radio map. (c)–(e) Corresponding images from the RadioMap3DSeer Dataset. (c) Pathloss radio map in the dataset after post-processing of simulation results shown in (b) and (d) Map of the buildings with their heights are encoded in gray levels. (e) BW city map.**

where $\tilde{\mathrm{P}}_{\mathrm{L}}^{(n)}$ and $\mathrm{P}_{\mathrm{L}}^{(n)}$ are the predicted and the ground truth radio maps, R and C are the number of rows and columns in a radio map image ($R = C = 256$ in our setting of RadioMap3DSeer Dataset), respectively.

VI. BASELINE METHOD

Our previously published work *RadioUNet* [3] and its publicly available code[3] were available for the participants as a baseline. Please see Section II-A3b for the description of RadioUNet$_C$, which is the relevant version of RadioUNet for the challenge.

VII. SUBMITTED METHODS

In the following, we describe the submitted methods. Most of the submitted methods are adaptations of the authors' previous work for the challenge, namely, the PMNet [89] and [81] are adaptations of the methods under the same name presented in [4] and [80], respectively, whereas the Agile method [84] incorporates a well-suited Kullback-Leibler (KL) divergence loss that was proposed by the authors in [100]. The detailed descriptions of the relevant previous work can be found in Section II-A3b.

A. AGILE RADIO MAP PREDICTION USING DEEP LEARNING [24], [84]

The proposed method adopts a UNet architecture and uses an additional input feature, namely, a fractional LOS map generated using Bresenham's line algorithm [121] and the CuPy library [85], which allow efficient GPU-accelerated computations. Furthermore, the authors use the Kullback-Leibler divergence loss function presented in [100] for uncertainty prediction, with the aim of reducing the effect of pixels with high uncertainty on the loss.

[3][Online]. Available: https://GitHub.com/RonLevie/RadioUNet

TABLE 2. Accuracies of the Submitted Methods on the Test Dataset $\mathcal{T}$. PPNet [81] Adopts a SegNet-Like Design. Agile [24], [84] is UNet Based and Takes an Additional Fractional LOS Map as Input. PMNet [89] Makes Use of ResBlocks, Dilated Convolutions, Skip Connections and Data Augmentation

Method	$\text{RMSE}_{\mathcal{T}}$
PPNet [81]	0.0507
Agile (MSE) [84]	0.0514
Agile (MSE, LOS) [84]	0.0461
Agile (KL, LOS) [84]	0.0451
PMNet ($\frac{H}{16} \times \frac{W}{16}$, w/ Fine Tuning) [89]	0.0959
PMNet ($\frac{H}{16} \times \frac{W}{16}$) [89]	0.0633
PMNet ($\frac{H}{8} \times \frac{W}{8}$) [89]	**0.0383**

B. PMNET: LARGE-SCALE CHANNEL PREDICTION SYSTEM FOR ICASSP 2023 FIRST PATHLOSS RADIO MAP PREDICTION CHALLENGE [89]

For this challenge, the authors adapted their previous pathloss map prediction network (PMNet) [4] with some modifications, such as adjusting the size of the feature map. The PMNet is an encoder-decoder DNN, where the encoder contains a series of ResBlock [90]. Similar to UNet [57], skip connections across the layers of the encoder and the decoder are employed. Moreover, PMNet uses atrous (dilated) convolutions with different rates [67], [91] and data augmentation.

C. DEEP LEARNING-BASED PATH LOSS PREDICTION FOR OUTDOOR WIRELESS COMMUNICATION SYSTEMS [81]

The authors presented a SegNet-like [82] fully convolutional encoder-decoder pathloss prediction network (PPNet) [80], where the pooling layers not only extract the largest values from the region of the feature map covered by the filter, but, unlike typical max-pooling, also the locations of the largest values, which are then used in the decoding phase.

VIII. CHALLENGE RESULTS

We summarize the accuracies of the submitted methods in Table 2 and show the prediction results for some samples from the test dataset in Fig. 3. Based on our evaluations and the declarations of the participants, a significant degradation of performance of all the submitted methods on the new test dataset was observed (with respect to testing on a hold-out subset of RadioMap3DSeer Dataset).

All participants reported run-times of about ∼10 ms, complying with the requirements of the challenge.

All the methods used the height-encoded city maps and Tx maps as input features. The use of the fractional LOS map as an additional input feature map proved to be useful, as shown by the results of the Agile method [84] (see the challenge follow-up paper [24] for more details).

We would like to note here that the RMSE calculations reported in [89] differ from the one explained here (2),(3) and in [81], [84]. The RMSE results presented in [89] were found by evaluating on a hold-out set of RadioMap3DSeer and seemingly by averaging of RMSEs calculated on mini-batches of size 16, and without setting the building pixels to zero. Also, we couldn't verify PMNet (w/ Fine Tuning) version to yield the given results in [89], as we observed worse performance also in the hold-out RadioMap3DSeer subset the authors apparently used. Nevertheless, the best performing setting of PMNet with the suitable choice of strides of the convolution, which leads to the output of the encoder to have size $\frac{H}{8} \times \frac{W}{8}$ (H and W are the height and width of an input image, $H = W = 256$ in our challenge setting), demonstrated a remarkable performance on the challenge test dataset, and ranked the first among all the methods.

IX. DISCUSSION AND FUTURE OUTLOOK

Visual inspection of the results in Fig. 3 shows that the best performing method, PMNet [89], has the most accurate shadow prediction of all the methods submitted. PMNet has three main features that differentiate it from other methods: the use of dilated convolutions, data augmentation, and ResBlocks. The results presented in PMNet [89] demonstrate the significant improvements in accuracy due to data augmentation and suggest that a significant amount of PMNet's superior performance can be attributed to it. Similarly, the results of the Agile method presented in [84] demonstrate the importance of another pre-processing in the form of generating an additional fractional LOS input feature. As can be seen in Fig. 3, this method demonstrates a higher long-range estimation accuracy with the use of LOS maps as an input feature map.

Therefore, to evaluate the performance of the neural networks alone, their contribution needs to be isolated by fixing other factors, such as the aforementioned very effective use of LOS maps as inputs or data augmentation. We hope that this will be addressed in future work and challenges.

APPENDIX
INTELLIGENT RAY TRACING (IRT) [48]

This method starts with a pre-processing step for the considered city map which allows to reduce the computation time for different Tx placements in the same propagation environment. In the pre-processing, the faces of the buildings are discretized into regular tiles, their edges into segments, and the visibility relations among the centers of these elements are found. For the visible element pairs, the distance between their centers and the subtended angles are calculated and stored. The result of the pre-processing of the city map is a tree structure comprising tiles, segments and receiving points of the prediction area of interest.

For prediction, only the tiles, segments and receiving points visible from the Tx position need to be determined. In addition, the angles of incidence for the tiles and segments that are visible have to be calculated. After that, a path between the Tx point and the receiving point can be found by recursively processing all the visible elements and checking if the specific conditions for reflection or diffraction are met. The search is stopped when a given maximum number of of interactions or a receiving point is reached. Finally, the sum of the field strength at all potential receiving points is calculated.

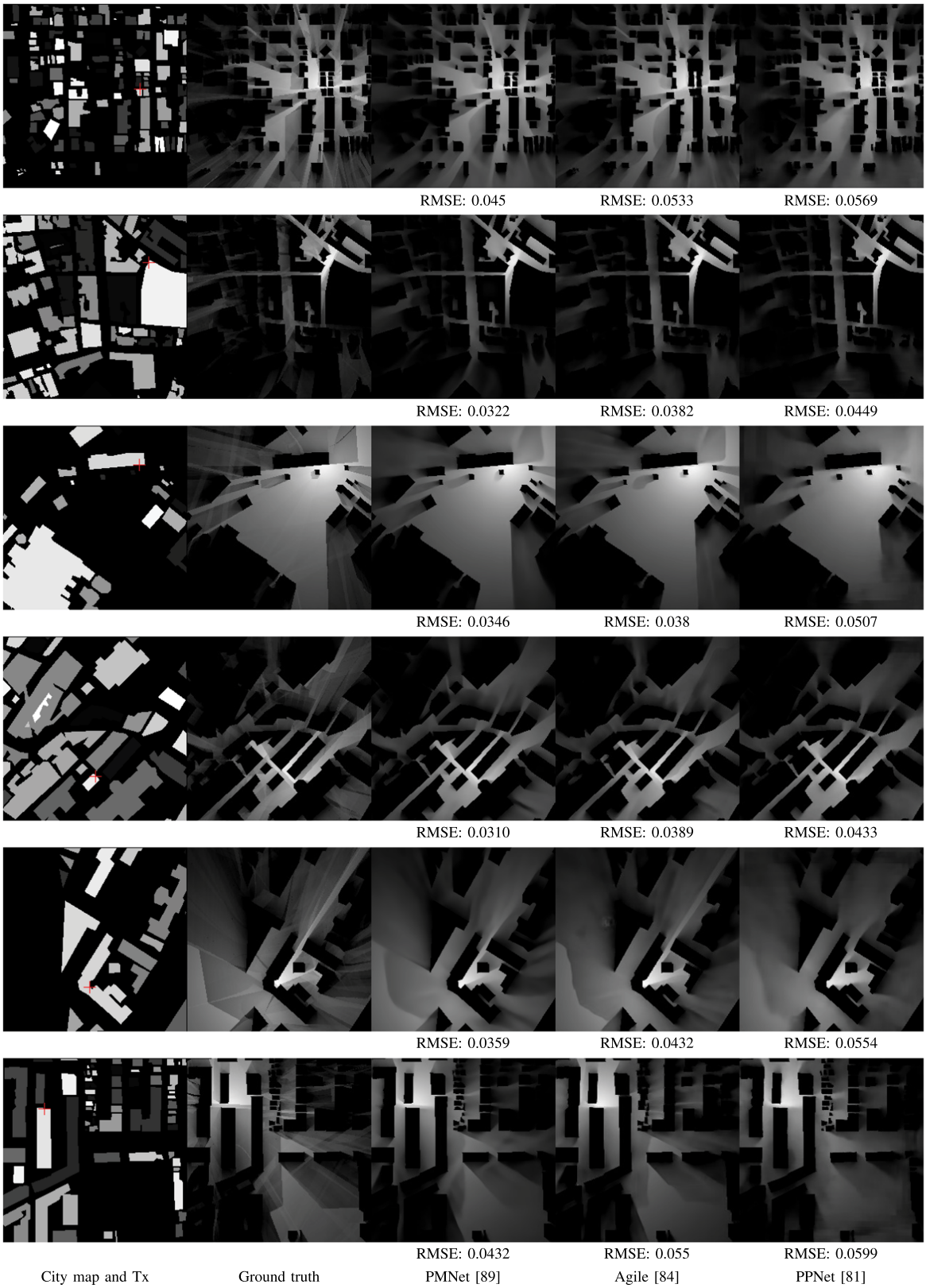

FIGURE 3. Examples from the test dataset. First column: height-encoded city map (the lighter the pixel, the taller the building) and Tx locations (shown with a red plus sign). Second column: ground truth simulation. Third to fifth columns: predictions of the successful methods and RMSEs. RMSEs of all the 6 examples: PMNet [89]: 0.0374, Agile [84]: 0.045, PPNet [81]: 0.0522.

Based on our experiments with different maximum numbers of interactions, we chose 2 interactions for its manageable computation times, which allowed us to prepare the dataset in a reasonable time, while the simulation results did not differ much from those with higher numbers of interactions. We set the length of the segments/tiles of the buildings to 10 meters, which, similarly as above, gave a good trade-off between computation time and richness of reflection patterns in the simulations.

REFERENCES

[1] Ç. Yapar, F. Jaensch, R. Levie, G. Kutyniok, and G. Caire, "The first pathloss radio map prediction challenge," in *Proc. IEEE Int. Conf. Acoust., Speech Signal Process.*, 2023, pp. 1–2.

[2] V. Raida, P. Svoboda, and M. Rupp, "On the inappropriateness of static measurements for benchmarking in wireless networks," in *Proc. IEEE 91st Veh. Technol. Conf.*, 2020, pp. 1–5.

[3] R. Levie, Ç. Yapar, G. Kutyniok, and G. Caire, "RadioUNet: Fast radio map estimation with convolutional neural networks," *IEEE Trans. Wireless Commun.*, vol. 20, no. 6, pp. 4001–4015, Jun. 2021.

[4] J.-H. Lee, O. G. Serbetci, D. P. Selvam, and A. F. Molisch, "PMNet: Robust pathloss map prediction via supervised learning," in *Proc. IEEE Glob. Commun. Conf.*, 2023, pp. 4601–4606.

[5] S. Zhang, A. Wijesinghe, and Z. Ding, "RME-GAN: A learning framework for radio map estimation based on conditional generative adversarial network," *IEEE Internet Things J.*, vol. 10, no. 20, pp. 18016–18027, Oct. 2023.

[6] A. Chaves-Villota and C. A. Viteri-Mera, "DeepREM: Deep-learning-based radio environment map estimation from sparse measurements," *IEEE Access*, vol. 11, pp. 48697–48714, 2023.

[7] D. Bethanabhotla, O. Y. Bursalioglu, H. C. Papadopoulos, and G. Caire, "Optimal user-cell association for massive MIMO wireless networks," *IEEE Trans. Wireless Commun.*, vol. 15, no. 3, pp. 1835–1850, Mar. 2016.

[8] N. Singh, S. Choe, and R. Punmiya, "Machine learning based indoor localization using Wi-Fi RSSI fingerprints: An overview," *IEEE Access*, vol. 9, pp. 127150–127174, 2021.

[9] Ç. Yapar, R. Levie, G. Kutyniok, and G. Caire, "LocUNet: Fast urban positioning using radio maps and deep learning," in *Proc. IEEE Int. Conf. Acoust., Speech Signal Process.*, 2022, pp. 4063–4067.

[10] Ç. Yapar, R. Levie, G. Kutyniok, and G. Caire, "Real-time outdoor localization using radio maps: A deep learning approach," *IEEE Trans. Wireless Commun.*, vol. 22, no. 12, pp. 9703–9717, Dec. 2023.

[11] T. V. Chien, T. N. Canh, E. Björnson, and E. G. Larsson, "Power control in cellular massive MIMO with varying user activity: A deep learning solution," *IEEE Trans. Wireless Commun.*, vol. 19, no. 9, pp. 5732–5748, Sep. 2020.

[12] Z. Utkovski, P. Agostini, M. Frey, I. Bjelakovic, and S. Stanczak, "Learning radio maps for physical-layer security in the radio access," in *Proc. IEEE Int. Workshop Signal Proc. Adv. Wireless Commun.*, 2019, pp. 1–5.

[13] Z. Chen, F. Sohrabi, and W. Yu, "Sparse activity detection for massive connectivity," *IEEE Trans. Signal. Process.*, vol. 66, no. 7, pp. 1890–1904, Apr. 2018.

[14] C.-H. Liu, H. Chang, and T. Park, "DA-cGAN: A framework for indoor radio design using a dimension-aware conditional generative adversarial network," in *Proc. IEEE/CVF Conf. Comput. Vis. Pattern Recognit. Workshops*, 2020, pp. 2089–2098.

[15] V. V. Ratnam et al., "FadeNet: Deep learning-based mm-wave large-scale channel fading prediction and its applications," *IEEE Access*, vol. 9, pp. 3278–3290, 2021.

[16] A. Seretis, C. Xu, and C. Sarris, "Fast selection of indoor wireless transmitter locations with generalizable neural network propagation models," *Inst. Elect. Electron. Eng.*, Oct. 2023, doi: 10.36227/techrxiv.24425536.v1.

[17] Y. Zheng, C. Liao, J. Wang, and S. Liu, "A transformer-based network for unifying radio map estimation and optimized site selection," in *Proc. IEEE Int. Conf. Acoustics, Speech, Signal Process. Workshops*, 2024.

[18] H. Li, P. Li, J. Xu, J. Chen, and Y. Zeng, "Derivative-free placement optimization for multi-UAV wireless networks with channel knowledge map," in *Proc. IEEE Int. Conf. Commun. Workshops*, 2022, pp. 1029–1034.

[19] X. Fang et al., "Radio map-based spectrum sharing for joint communication and sensing," *IEEE Open J. Commun. Soc.*, p. 1, 2024.

[20] L. Zhang, H. Sun, J. Sun, R. Parasuraman, Y. Ye, and R. Q. Hu, "Map2Schedule: An end-to-end link scheduling method for urban V2V communications," 2023, *arXiv:2310.08364*.

[21] W. Feng et al., "Radio map-based cognitive satellite-UAV networks towards 6G on-demand coverage," *IEEE Trans. Cogn. Commun. Netw.*, vol. 10, no. 3, pp. 1075–1089, Jun. 2024.

[22] T. N. Ha, D. Romero, and R. López-Valcarce, "Radio maps for beam alignment in mmWave communications with location uncertainty," 2024, *arXiv:2402.16156*.

[23] S. Zhang and R. Zhang, "Radio map based path planning for cellular-connected UAV," in *Proc. IEEE Glob. Commun. Conf.*, 2019, pp. 1–6.

[24] H. Sallouha, S. Sarkar, E. Krijestorac, and D. Cabric, "REM-U-Net: Deep learning based agile REM prediction with energy-efficient cell-free use case," *IEEE Open J. Signal Process.*, vol. 5, pp. 750–765, 2024.

[25] Z. Li, J. Cao, H. Wang, and M. Zhao, "Sparsely self-supervised generative adversarial nets for radio frequency estimation," *IEEE J. Sel. Areas Commun.*, vol. 37, no. 11, pp. 2428–2442, Nov. 2019.

[26] R. Levie, Ç. Yapar, G. Kutyniok, and G. Caire, "Pathloss prediction using deep learning with applications to cellular optimization and efficient D2D link scheduling," in *Proc. IEEE Int. Conf. Acoust., Speech Signal Process.*, 2020, pp. 8678–8682.

[27] X. Zhang, X. Shu, B. Zhang, J. Ren, L. Zhou, and X. Chen, "Cellular network radio propagation modeling with deep convolutional neural networks," in *Proc. 26th ACM SIGKDD Int. Conf. Knowl. Discov. Data Mining*, 2020, pp. 2378–2386.

[28] C. Yapar, R. Levie, G. Kutyniok, and G. Caire, "Dataset of pathloss and ToA radio maps with localization application," *IEEE Dataport*, 2022, [Online]. Available: https://dx.doi.org/10.21227/0gtx-6v30

[29] Ç. Yapar, R. Levie, G. Kutyniok, and G. Caire, "Dataset of pathloss and ToA radio maps with localization application," 2022, *arXiv:2212.11777*.

[30] T. Sarkar, Z. Ji, K. Kim, A. Medouri, and M. Salazar-Palma, "A survey of various propagation models for mobile communication," *IEEE Antennas Propag. Mag.*, vol. 45, no. 3, pp. 51–82, Jun. 2003.

[31] C. Phillips, D. Sicker, and D. Grunwald, "A survey of wireless path loss prediction and coverage mapping methods," *IEEE Commun. Surv. Tuts.*, vol. 15, no. 1, pp. 255–270, Firstquarter 2013.

[32] A. F. Molisch, *Wireless Communications*, vol. 34. Hoboken, NJ, USA: Wiley, 2012.

[33] M. Hata, "Empirical formula for propagation loss in land mobile radio services," *IEEE Trans. Veh. Technol.*, vol. VT-29, no. 3, pp. 317–325, Aug. 1980.

[34] P. Mogensen and J. Wigard, *COST Action 231: Digital Mobile Radio Towards Future Generation System, Final Report*. Brussels, Belgium: European Commission, 1999.

[35] K. Hari, D. Baum, A. Rustako, R. Roman, and D. Trinkwon, "Channel models for fixed wireless applications," IEEE 802.16 Broadband Wireless Access Working Group, 2003.

[36] Forsk, "Atoll 3.3. 0 technical reference guide for radio networks," 1997.

[37] S. Jaeckel, L. Raschkowski, K. Börner, and L. Thiele, "QuaDRiGa: A 3-D multi-cell channel model with time evolution for enabling virtual field trials," *IEEE Trans. Antennas Propag.*, vol. 62, no. 6, pp. 3242–3256, Jun. 2014.

[38] Z. Yun and M. F. Iskander, "Ray tracing for radio propagation modeling: Principles and applications," *IEEE Access*, vol. 3, pp. 1089–1100, 2015.

[39] S. Hagness, A. Taflove, and S. Gedney, "Finite-difference time-domain methods: Numerical methods in electromagnetics," in *Handbook of Numerical Analysis: Numerical Methods in Electromagnetics*. Amsterdam, The Netherlands: Elsevier North Holland, 2005, pp. 199–315.

[40] S. Sarkar, M. H. Manshaei, and M. Krunz, "RADIANCE: Radio-frequency adversarial deep-learning inference for automated network coverage estimation," in *Proc. IEEE Glob. Commun. Conf.*, 2023, pp. 832–837.

[41] F. Jaensch, G. Caire, and B. Demir, "Radio map estimation–an open dataset with directive transmitter antennas and initial experiments," 2024, *arXiv:2402.00878*.

[42] F. Zhang et al., "A radio wave propagation modeling method based on high precision 3D mapping in urban scenarios," *IEEE Trans. Antennas Propag.*, vol. 72, no. 3, pp. 2712–2722, Mar. 2024.

[43] R. Hoppe, G. Wölfle, and U. Jakobus, "Wave propagation and radio network planning software WinProp added to the electromagnetic solver package FEKO," in *Proc. IEEE Int. Appl. Comput. Electromagnetics Soc. Symp.*, 2017, pp. 1–2.

[44] H. Ling, R.-C. Chou, and S.-W. Lee, "Shooting and bouncing rays: Calculating the RCS of an arbitrarily shaped cavity," *IEEE Trans. Antennas Propag.*, vol. 37, no. 2, pp. 194–205, Feb. 1989.

[45] G. Liang and H. Bertoni, "A new approach to 3-D ray tracing for propagation prediction in cities," *IEEE Trans. Antennas Propag.*, vol. 46, no. 6, pp. 853–863, Jun. 1998.

[46] D. He, B. Ai, K. Guan, L. Wang, Z. Zhong, and T. Kürner, "The design and applications of high-performance ray-tracing simulation platform for 5G and beyond wireless communications: A tutorial," *IEEE Commun. Surv. Tuts.*, vol. 21, no. 1, pp. 10–27, Firstquarter 2019.

[47] R. Wahl, G. Wölfle, P. Wertz, P. Wildbolz, and F. Landstorfer, "Dominant path prediction model for urban scenarios," in *Proc. 14th IST Mobile Wireless Commun. Summit*, 2005, pp. 1–5.

[48] R. Hoppe, G. Wölfle, and F. Landstorfer, "Fast 3-D ray tracing for the planning of microcells by intelligent preprocessing of the data base," in *Proc. 3rd Eur. Pers. Mobile Commun. Conf.*, 1999, pp. 149–154.

[49] J. M. Keenan and A. J. Motley, "Radio coverage in buildings," *Brit. Telecom Technol. J.*, vol. 8, no. 1, pp. 19–24, 1990.

[50] S. Hosseinzadeh, H. Larijani, K. Curtis, A. Wixted, and A. Amini, "Empirical propagation performance evaluation of LoRa for indoor environment," in *Proc. IEEE 15th Int. Conf. Ind. Informat.*, 2017, pp. 26–31.

[51] T. Imai, K. Kitao, and M. Inomata, "Radio propagation prediction model using convolutional neural networks by deep learning," in *Proc. IEEE Eur. Conf. Antennas Propag.*, 2019, pp. 1–5.

[52] K. Saito, Y. Jin, C. Kang, J. Takada, and J.-S. Leu, "Two-step path loss prediction by artificial neural network for wireless service area planning," *IEICE Commun. Exp.*, vol. 8, no. 12, pp. 611–616, 2019.

[53] S. I. Popoola et al., "Determination of neural network parameters for path loss prediction in very high frequency wireless channel," *IEEE Access*, vol. 7, pp. 150462–150483, 2019.

[54] S. P. Sotiroudis and K. Siakavara, "Mobile radio propagation path loss prediction using artificial neural networks with optimal input information for urban environments," *AEU-Int. J. Electron. Commun.*, vol. 69, no. 10, pp. 1453–1463, 2015.

[55] S. P. Sotiroudis, S. K. Goudos, K. A. Gotsis, K. Siakavara, and J. N. Sahalos, "Application of a composite differential evolution algorithm in optimal neural network design for propagation path-loss prediction in mobile communication systems," *IEEE Antennas Wireless Propag. Lett.*, vol. 12, pp. 364–367, 2013.

[56] J. M. Mom, C. O. Mgbe, and G. A. Igwue, "Application of artificial neural network for path loss prediction in urban macrocellular environment," *Amer. J. Eng. Res*, vol. 3, no. 2, pp. 270–275, 2014.

[57] O. Ronneberger, P. Fischer, and T. Brox, "U-Net: Convolutional networks for biomedical image segmentation," in *Proc. Med. Image Comput. Comput.-Assisted Intervention*, 2015, pp. 234–241.

[58] S. Bakirtzis, J. Chen, K. Qiu, J. Zhang, and I. Wassell, "EM DeepRay: An expedient, generalizable, and realistic data-driven indoor propagation model," *IEEE Trans. Antennas Propag.*, vol. 70, no. 6, pp. 4140–4154, Jun. 2022.

[59] A. Doshi, J. Namgoong, and T. Yoo, "Radio DIP - completing radio maps using deep image prior," in *Proc. IEEE Glob. Commun. Conf.*, 2023, pp. 1543–1548.

[60] S. J. Pan and Q. Yang, "A survey on transfer learning," *IEEE Trans. Knowl. Data Eng.*, vol. 22, no. 10, pp. 1345–1359, Oct. 2010.

[61] Y. Li, Z. Li, Z. Gao, and T. Chen, "Geo2sigmap: High-fidelity RF signal mapping using geographic databases," 2023, *arXiv:2312.14303*.

[62] J.-H. Lee and A. F. Molisch, "A scalable and generalizable pathloss map prediction," 2023, *arXiv:2312.03950*.

[63] A. Marey, M. Bal, H. F. Ates, and B. K. Gunturk, "PL-GAN: Path loss prediction using generative adversarial networks," *IEEE Access*, vol. 10, pp. 90474–90480, 2022.

[64] M. R. Ziemann, J. S. Hyatt, and M. S. Lee, "Convolutional neural networks for radio frequency ray tracing," in *Proc. IEEE Mil. Commun. Conf.*, 2021, pp. 618–622.

[65] S. Xie, R. Girshick, P. Dollar, Z. Tu, and K. He, "Aggregated residual transformations for deep neural networks," in *Proc. IEEE Conf. Comput. Vis. Pattern Recognit.*, 2017, pp. 5987–5995.

[66] M. Holschneider, R. Kronland-Martinet, J. Morlet, and P. Tchamitchian, "A real-time algorithm for signal analysis with the help of the wavelet transform," in *Proc. Wavelets*, 1989, pp. 286–297.

[67] F. Yu and V. Koltun, "Multi-scale context aggregation by dilated convolutions," 2015, *arXiv:1511.07122*.

[68] S. Bakirtzis, K. Qiu, J. Zhang, and I. Wassell, "DeepRay: Deep learning meets ray-tracing," in *Proc. IEEE 16th Eur. Conf. Antennas Propag.*, 2022, pp. 1–5.

[69] C. T. Cisse, O. Baala, V. Guillet, F. Spies, and A. Caminada, "IRGAN: CGAN-based indoor radio map prediction," in *Proc. IEEE IFIP Netw. Conf.*, 2023, pp. 1–9.

[70] Y. Tian, S. Yuan, W. Chen, and N. Liu, "Transformer based radio map prediction model for dense urban environments," in *Proc. IEEE 13th Int. Symp. Antennas, Propag. EM Theory*, 2021, pp. 1–3.

[71] Y. Tian, S. Yuan, W. Chen, and N. Liu, "Radionet: Transformer based radio map prediction model for dense urban environments," 2021, *arXiv:2105.07158*.

[72] A. Vaswani et al., "Attention is all you need," in *Proc. Adv. Neural Inf. Process. Syst.*, 2017, pp. 5998–6008.

[73] A. Dosovitskiy et al., "An image is worth 16×16 words: Transformers for image recognition at scale," 2020, *arXiv:2010.11929*.

[74] Ç. Yapar, "Deep learning-based pathloss radio map estimation and its application to RSS fingerprint-based localization," Doctoral Thesis, Technische Universität Berlin, 2023.

[75] O. Ozyegen, S. Mohammadjafari, M. Cevik, K. El Mokhtari, J. Ethier, and A. Basar, "An empirical study on using CNNs for fast radio signal prediction," *SN Comput. Sci.*, vol. 3, no. 2, 2022, Art. no. 131.

[76] J. Springenberg, A. Dosovitskiy, T. Brox, and M. Riedmiller, "Striving for simplicity: The all convolutional net," 2014, *arXiv:1412.6806*.

[77] C. Szegedy et al., "Going deeper with convolutions," in *Proc. IEEE Conf. Comput. Vis. Pattern Recognit.*, 2015, pp. 1–9.

[78] M. Chen, M. Châteauvert, and J. Ethier, "Extending machine learning based RF coverage predictions to 3D," in *Proc. IEEE Int. Symp. Antennas Propag. USNC-URSI Radio Sci. Meeting*, 2022, pp. 205–206.

[79] B. S. Shawel, D. H. Woldegebreal, and S. Pollin, "A deep-learning approach to a volumetric radio environment map construction for UAV-assisted networks," *Int. J. Antennas Propag.*, vol. 2024, pp. 1–16, 2024.

[80] K. Qiu, S. Bakirtzis, H. Song, J. Zhang, and I. Wassell, "Pseudo ray-tracing: Deep leaning assisted outdoor mm-wave path loss prediction," *IEEE Wireless Commun. Lett.*, vol. 11, no. 8, pp. 1699–1702, Aug. 2022.

[81] K. Qiu, S. Bakirtzis, H. Song, I. Wassell, and J. Zhang, "Deep learning-based path loss prediction for outdoor wireless communication systems," in *Proc. IEEE Int. Conf. Acoust., Speech Signal Process.*, 2023, pp. 1–2.

[82] V. Badrinarayanan, A. Kendall, and R. Cipolla, "SegNet: A deep convolutional encoder-decoder architecture for image segmentation," *IEEE Trans. Pattern Anal. Mach. Intell.*, vol. 39, no. 12, pp. 2481–2495, Dec. 2017.

[83] 3GPP TR 38.901, "Study on channel model for frequencies from 0.5 to 100 GHz.," *3rd Generation Partnership Project*, 3GPP Sophia Antipolis, France, 2017.

[84] E. Krijestorac, H. Sallouha, S. Sarkar, and D. Cabric, "Agile radio map prediction using deep learning," in *Proc. IEEE Int. Conf. Acoust., Speech Signal Process.*, 2023, pp. 1–2.

[85] R. Okuta, Y. Unno, D. Nishino, and S. Hido, and C. Loomis, "CuPy: A NumPy-compatible library for NVIDIA GPU calculations," in *Proc. 31st Conf. Neural Inf. Process. Syst.*, 2017. [Online]. Available: http://learningsys.org/nips17/assets/papers/paper_16.pdf

[86] Y. Zeng et al., "A tutorial on environment-aware communications via channel knowledge map for 6G," *IEEE Commun. Surv. Tuts.*, early access, Feb. 09, 2024, doi: 10.1109/COMST.2024.3364508.

[87] P. Agrawal and N. Patwari, "Correlated link shadow fading in multi-hop wireless networks," *IEEE Trans. Wireless Commun.*, vol. 8, no. 8, pp. 4024–4036, Aug. 2009.

[88] Z. Tan, Z. Yao, L. Xiao, M. Zhao, and Y. Li, "A new approach to predict radio map via learning-based spatial loss field," in *Proc. IEEE Int. Conf. Acoustics, Speech, Signal Process. Workshops*, 2024.
[89] J.-H. Lee, J. Lee, S.-H. Lee, and A. F. Molisch, "PMNet: Large-scale channel prediction system for ICASSP 2023 first pathloss radio map prediction challenge," in *Proc. IEEE Int. Conf. Acoust., Speech Signal Process.*, 2023, pp. 1–2.
[90] K. He, X. Zhang, S. Ren, and J. Sun, "Deep residual learning for image recognition," in *Proc. IEEE Conf. Comput. Vis. Pattern Recognit.*, 2016, pp. 770–778.
[91] L.-C. Chen, Y. Zhu, G. Papandreou, F. Schroff, and H. Adam, "Encoder-decoder with atrous separable convolution for semantic image segmentation," in *Proc. Eur. Conf. Comput. Vis.*, 2018, pp. 801–818.
[92] G. Femenias, N. Lassoued, and F. Riera-Palou, "Access point switch ON/OFF strategies for green cell-free massive MIMO networking," *IEEE Access*, vol. 8, pp. 21788–21803, 2020.
[93] J. Dai et al., "Deformable convolutional networks," in *Proc. IEEE Int. Conf. Comput. Vis.*, 2017, pp. 764–773.
[94] M. Mirza and S. Osindero, "Conditional generative adversarial nets," 2014, *arXiv:1411.1784*.
[95] S. K. Vankayala, S. Kumar, I. Roy, D. Thirumulanathan, S. Yoon, and I. S. Kanakaraj, "Radio map estimation using a generative adversarial network and related business aspects," in *Proc. IEEE 24th Int. Symp. Wireless Pers. Multimedia Commun.*, 2021, pp. 1–6.
[96] P. Isola, J.-Y. Zhu, T. Zhou, and A. A. Efros, "Image-to-image translation with conditional adversarial networks," in *Proc. IEEE Conf. Comput. Vis. Pattern Recognit.*, 2017, pp. 1125–1134.
[97] S. Kasdorf, B. Troksa, C. Key, J. Harmon, S. Pasricha, and B. M. Notaroš, "Parallel GPU optimization of the shooting and bouncing ray tracing methodology for propagation modeling," *IEEE Trans. Antennas Propag.*, vol. 72, no. 1, pp. 174–182, Jan. 2024.
[98] Y. Teganya and D. Romero, "Deep completion autoencoders for radio map estimation," *IEEE Trans. Wireless Commun.*, vol. 21, no. 3, pp. 1710–1724, Mar. 2022.
[99] W. Locke, N. Lokhmachev, Y. Huang, and X. Li, "Radio map estimation with deep dual path autoencoders and skip connection learning," in *Proc. IEEE 34th Annu. Int. Symp. Pers., Indoor Mobile Radio Commun.*, 2023, pp. 1–6.
[100] E. Krijestorac, S. Hanna, and D. Cabric, "Spatial signal strength prediction using 3D maps and deep learning," in *Proc. IEEE Int. Conf. Commun.*, 2021, pp. 1–6.
[101] M. Mallik, B. Allaert, A. Tesfay, D. Gaillot, J. Wiart, and L. Clavier, "EME-GAN: A conditional generative adversarial network based indoor EMF exposure map reconstruction," in *Proc. 29Â Colloque sur le traitement du signal et des image*, 2023, pp. 745–748.
[102] M. Mallik et al., "EME-Net: A U-net-based indoor EMF exposure map reconstruction method," in *Proc. IEEE 16th Eur. Conf. Antennas Propag.*, 2022, pp. 1–5.
[103] C. Qi, Y. Jingjing, H. Ming, and Z. Qiang, "ACT-GAN: Radio map construction based on generative adversarial networks with ACT blocks," 2024, *arXiv:2401.08976*.
[104] S. Woo, J. Park, J.-Y. Lee, and I. S. Kweon, "CBAM: Convolutional block attention module," in *Proc. Eur. Conf. Comput. Vis.*, 2018, pp. 3–19.
[105] Y. Zeng, J. Fu, H. Chao, and B. Guo, "Aggregated contextual transformations for high-resolution image inpainting," *IEEE Trans. Vis. Comput. Graph.*, vol. 29, no. 7, pp. 3266–3280, Jul. 2023.
[106] Z. Zhang, G. Zhu, J. Chen, and S. Cui, "Fast and accurate cooperative radio map estimation enabled by GAN," 2024, *arXiv:2402.02729*.
[107] C. M. Bishop, *Neural Networks for Pattern Recognition*. New York, NY, USA: Oxford Univ. Press, Inc., 1995.
[108] W. C. Van Beers and J. P. Kleijnen, "Kriging interpolation in simulation: A survey," in *Proc. IEEE Winter Simul. Conf.*, 2004, pp. 113–121.
[109] D. Schäufele, R. L. G. Cavalcante, and S. Stanczak, "Tensor completion for radio map reconstruction using low rank and smoothness," in *Proc. IEEE 20th Int. Workshop Signal Process. Adv. Wireless Commun.*, 2019, pp. 1–5.
[110] Y. Zhang and S. Wang, "K-nearest neighbors gaussian process regression for urban radio map reconstruction," *IEEE Commun. Lett.*, vol. 26, no. 12, pp. 3049–3053, Dec. 2022.
[111] D. Romero and S.-J. Kim, "Radio map estimation: A. data-driven approach to spectrum cartography," *IEEE Signal Process. Mag.*, vol. 39, no. 6, pp. 53–72, Nov. 2022.
[112] M. Pesko, T. Javornik, A. Kosir, M. Stular, and M. Mohorcic, "Radio environment maps: The survey of construction methods," *KSII Trans. Internet Inf. Syst.*, vol. 8, no. 11, pp. 3789–3809, 2014.
[113] M. Torun, H. Cai, and Y. Mostofi, "Spatial prediction of channel signal strength map using deep fully convolutional neural network," in *Proc. IEEE 56th Asilomar Conf. Signals, Syst., Comput.*, 2022, pp. 553–558.
[114] M. Malmirchegini and Y. Mostofi, "On the spatial predictability of communication channels," *IEEE Trans. Wireless Commun.*, vol. 11, no. 3, pp. 964–978, Mar. 2012.
[115] S. Shrestha, X. Fu, and M. Hong, "Deep spectrum cartography: Completing radio map tensors using learned neural models," *IEEE Trans. Signal Process.*, vol. 70, pp. 1170–1184, 2022.
[116] K. Qiu, S. Bakirtzis, I. Wassell, H. Song, K. Lin, and J. Zhang, "IRDM: A. generative diffusion model for indoor radio map interpolation," in *Proc. IEEE Glob. Commun. Conf.*, 2023, pp. 1–6.
[117] L. Yang et al., "Diffusion models: A. comprehensive survey of methods and applications," *ACM Comput. Surv.*, vol. 56, no. 4, pp. 1–39, 2023.
[118] OpenStreetMap contributors, "Planet dump retrieved from https://planet.osm.org," 2017. [Online]. Available: https://www.openstreetmap.org
[119] G. Wölfle, R. Hoppe, and F. M. Landstorfer, "A fast and enhanced ray optical propagation model for indoor and urban scenarios, based on an intelligent preprocessing of the database," in *Proc. 10th IEEE Int. Symp. Pers., Indoor Mobile Radio Commun.*, 1999.
[120] I. Stepanov and K. Rothermel, "On the impact of a more realistic physical layer on MANET simulations results," *Ad Hoc Netw.*, vol. 6, no. 1, pp. 61–78, 2008.
[121] J. E. Bresenham, "Algorithm for computer control of a digital plotter," *IBM Syst. J.*, vol. 4, no. 1, pp. 25–30, 1965.

ÇAĞKAN YAPAR (Member, IEEE) received the B.Sc. degree in electrical and electronics engineering from Boğaziçi University, Istanbul, Türkiye, in 2012, the M.Sc. degree in electrical engineering and information technology from the TU München, Munich, Germany, in 2015, and the Dr.-Ing. degree in electrical engineering and computer science from the TU Berlin, Berlin, Germany, in 2023. His research interests include machine learning, information theory, communications, and signal processing.

FABIAN JAENSCH received the M.Sc. degree in mathematics from Technische Universität Berlin, Berlin, Germany, in 2021. Since 2022, he has been a Doctoral Researcher with the Communications and Information Theory Chair, Technische Universität Berlin. His research interests include machine learning, computer vision, and applications to telecommunications.

RON LEVIE received the Ph.D. degree in applied mathematics from Tel Aviv University, Tel Aviv, Israel, in 2018. During 2018–2020, he was a Postdoctoral Researcher with the Institute of Mathematics, Technical University Berlin, Berlin, Germany. During 2021–2022, he was a Postdoctoral Researcher with the Department of Mathematics, Ludwig Maximilian University of Munich, Munich, Germany. Since 2022, he has been an Assistant Professor (Senior Lecturer) with the Faculty of Mathematics, Technion - Israel Institute of Technology, Haifa, Israel. His research interests include theory of deep learning, geometric deep learning, explainability of deep learning, signal processing, and applied harmonic analysis.

GITTA KUTYNIOK (Fellow, IEEE) received the diploma in mathematics and computer science and the Ph.D. degree from Universität Paderborn, Paderborn, Germany, and the Habilitation in mathematics from the Justus-Liebig Universität Gießen, Giessen, Germany, in 2006. From 2001 to 2008, she held visiting positions with several US institutions, such as Princeton University, Princeton, NJ, USA, Stanford University, Stanford, CA, USA, Yale University, New Haven, CT, USA, Georgia Institute of Technology, Atlanta, GA, USA, and Washington University in St. Louis, St. Louis, MO, USA. In 2008, she became a Full Professor of mathematics with the Universität Osnabrück, Osnabrück, Germany, and moved to Berlin three years later, where she held an Einstein Chair with the Institute of Mathematics, Technische Universität Berlin, Berlin, Germany, and a courtesy appointment with the Department of Computer Science and Engineering until 2020. In addition, she holds an Adjunct Professorship of machine learning with the University of Tromso, Tromso, Norway, since 2019. She currently has a Bavarian AI Chair for Mathematical Foundations of artificial intelligence, Ludwig-Maximilians-Universität München, Munich, Germany. Her research interests include the areas of applied and computational harmonic analysis, artificial intelligence, compressed sensing, deep learning, imaging sciences, inverse problems, and applications to life sciences, robotics, and telecommunication.

She was the recipient of various awards for her research, such as award from the Universität Paderborn in 2003, Research Prize of the Justus-Liebig Universität Gießen and a Heisenberg-Fellowship in 2006, and von Kaven Prize by the DFG in 2007. She was invited as the Noether Lecturer at the ÖMG-DMV Congress in 2013, plenary lecturer at the 8th European Congress of Mathematics (8ECM) in 2021, and lecturer of the London Mathematical Society (LMS) Invited Lecture Series in 2022. She was also honored by invited lectures at both the International Congress of Mathematicians 2022 (ICM 2022) and International Congress on Industrial and Applied Mathematics (ICIAM 2023). She was also elected as a Member of the Berlin-Brandenburg Academy of Sciences and Humanities in 2017 and of the European Academy of Sciences in 2022, and became a SIAM Fellow in 2019 as well as an IEEE Fellow in 2024. She is the LMU-Director of the Konrad Zuse School of Excellence in Reliable AI (relAI) in Munich and is the spokesperson for both the DFG-Priority Program "Theoretical Foundations of Deep Learning" and the AI-HUB@LMU, which is a transdisciplinary platform across all faculties of LMU for research, teaching, and transfer in the area of AI and data science.

GIUSEPPE CAIRE (Fellow, IEEE) was born in Torino, in 1965. He received the B.Sc. degree in electrical engineering from Politecnico di Torino, Turin, Italy, in 1990, the M.Sc. degree in electrical engineering from Princeton University, Princeton, NJ, USA, in 1992, and the Ph.D. degree from Politecnico di Torino, in 1994. He was a Postdoctoral Research Fellow with the European Space Agency (ESTEC) Noordwijk, The Netherlands, in 1994–1995, Assistant Professor of telecommunications with the Politecnico di Torino, Associate Professor with the University of Parma, Parma, Italy, Professor with the Department of Mobile Communications, Eurecom Institute, Sophia-Antipolis, France, Professor of electrical engineering with the Viterbi School of Engineering, University of Southern California, Los Angeles, CA, USA. He is currently an Alexander von Humboldt Professor with the Faculty of Electrical Engineering and Computer Science, Technical University of Berlin, Berlin, Germany. His main research interests include the field of communications theory, information theory, channel and source coding with particular focus on wireless communications.

He was the recipient of the Jack Neubauer Best System Paper Award from the IEEE Vehicular Technology Society in 2003, IEEE Communications Society and Information Theory Society Joint Paper Award in 2004 and in 2011, Okawa Research Award in 2006, Alexander von Humboldt Professorship in 2014, Vodafone Innovation Prize in 2015, ERC Advanced Grant in 2018, Leonard G. Abraham Prize for best IEEE JSAC paper in 2019, IEEE Communications Society Edwin Howard Armstrong Achievement Award in 2020, and 2021 Leibniz Prize of the German National Science Foundation (DFG). He was in the Board of Governors of the IEEE Information Theory Society from 2004 to 2007, and as Officer from 2008 to 2013. He was the President of the IEEE Information Theory Society in 2011.